

Thresholds for Data Compression by multi-scale Representation of Signals

Schwellen für die Datenkompression durch die Multi-Skalen-Repräsentation von Signalen

Karl-Rudolf Koch

Aus der automatischen Aufzeichnung von Daten ergibt sich die Notwendigkeit der Datenkompression. Eine allgemeine Methode folgt aus der Multi-Skalen-Repräsentation von Signalen. B-Spline-Flächen, auch als Freiformflächen bezeichnet, werden für die Darstellung angewendet. Eine effiziente Methode, um B-Spline-Flächen an Messungen anzupassen, erhält man mit der sogenannten Lofting-Methode. Die Multi-Skalen-Repräsentation von Punkten auf der angepassten Fläche mit einer Dichte, die höher ist als die der Messungen, wird abgeleitet. Kleine Wavelet-Koeffizienten dieser Darstellung können für eine Datenkompression eliminiert werden. Als Schwellen zur Vernachlässigung der Wavelet-Koeffizienten dienen ihre Konfidenzgrenzen, die mit Monte-Carlo-Verfahren berechnet werden. Falls Monte-Carlo-Methoden nicht praktikabel sind, werden die Schwellen durch die maximalen Absolutwerte der Wavelet-Koeffizienten zusammen mit der Standardabweichung, mit der die B-Spline-Fläche an die gemessenen Höhen angepasst wird, und mit den mittleren quadratischen Differenzen der Höhen der Flächen bestimmt, die mit und ohne Datenkompression berechnet werden. Diese Methoden werden für ein Beispiel erläutert, bei dem eine B-Spline-Fläche an die Koordinaten, gemessen mit einem Laserscanner, von Punkten auf einem Betonträger unter einer Kellerdecke angepasst wird.

SCHLÜSSELWÖRTER: B-Spline-Fläche, Detailsignal, Wavelet-Funktion, Lofting-Methode, Laserscanner

With the advent of automatic collection of data, the need of data compression arises. A general method is obtained by the multi-scale representation of signals. B-spline surfaces, also called free-form surfaces, are applied for the representation. An efficient method for fitting B-spline surfaces to measurements is given by the lofting method. The multi-scale representation of points on the fitted surface with a density higher than that of the measurements is derived. Small wavelet coefficients of this representation can be neglected to achieve data compression. Confidence intervals for the wavelet coefficients computed by Monte Carlo methods serve as thresholds for neglecting the wavelet coefficients. In case Monte Carlo simulations are not feasible, thresholds are established by the maximum absolute values of the wavelet coefficients together with the standard deviation, with which the B-spline surface is fitted to the measured heights, and with the root mean square difference between the heights of the surface computed with and without data compression. These methods are demonstrated by fitting a B-spline surface to the coordinates of points on a concrete beam under a ceiling measured by a laser scanner.

KEYWORDS: B-spline surface, detail signal, wavelet function, lofting method, laser scanner

1 INTRODUCTION

Data compression is a task which is routinely applied for digital signals. The best known example is the special compression for digital images stored in the jpg-format. A general method for data compression is available by the multi-scale representation of signals. At a lower level of resolution, a signal is computed by a low-pass filter. The difference of information in comparison to the original representation of the signal is obtained by the so-called detail signals which result from a wavelet representation. The detail signals are computed by band-pass filters with frequency bands resulting from the resolution level. The low-pass filtered version of the signal plus the detail signals gives the original signal. Some of the wavelet coefficients determining the detail signals will be small so that they can be neglected, thus achieving data compression.

The multi-scale representation of signals goes back to Mallat (1989). Schmidt (2001) presents geodetic applications, for instance, the multi-scale representation using Daubechies wavelet functions for digital image analysis and data compression. Quak and Weyrich (1994) based on Chui and Quak (1992) introduce spline wavelets. Stollnitz et al. (1995a,b) use endpoint-interpolating B-spline wavelets which are also applied here. They propose the tensor product for a the multi-scale representation of surfaces.

The tensor product of B-splines in two dimensions gives the well known free-form surfaces with many applications. For instance in reverse engineering, a B-spline surface is fitted to the measured coordinates of a manufactured object to obtain an analytical model which is modified by computer aided design, cf. Yang and Qian (2007). To correct for offsets of reflectors, free-form surfaces are applied by Hennes (2009). Three-dimensional models with high resolution, for instance of buildings, depicted by digital images are derived by free-form surfaces (Koch, 2011b). Fitting these surfaces to objects can be accomplished with an uncertainty which does not surpass the uncertainty of the measurements as was shown by Monte Carlo simulations (Koch, 2009c). By generalizing the tensor product of B-splines to three dimensions, surfaces of objects, which change with time and are measured, for instance, in a deformation analysis, can be represented by B-spline surfaces (Koch, 2010a). To model the electron density of the ionosphere, Schmidt et al. (2008) defined a four-dimensional B-spline surface. A numerical example of a four-dimensional surface is given by Koch and Schmidt (2011).

If the coordinates which are measured for representing an object are arranged in regular grids, the control points of the B-spline surface can be estimated by the so-called lofting method. It is much faster than the simultaneous estimation of the control points and should be preferred in case of many control points. The equivalence of the estimation is proved for two-dimensional B-spline surfaces by Koch (2009a) and holds also for n-dimensional ones (Koch and Schmidt, 2011).

Fitting B-spline surfaces to objects with discontinuities like edges needs a high density of the measurements. Outside the discontinuities, the high density is not necessary but it is fixed for an automatic measuring process like laser scanning. Examples are facades of buildings where a high density of the measurements is mandatory because of the windows and doors. Large parts of the facade are plane where the high density is not needed. Data compression is therefore recommended (Koch, 2011b).

An overview of the n-dimensional multi-scale representation of signals by B-spline surfaces is presented by Zeilhofer (2008) and Schmidt (2010). Koch (2011a) gives the details of deriving the decomposition equations and the n-dimensional multi-scale representation of signals with higher density than that of the measurements. To achieve data compression, small wavelet coefficients determining the detail signals are neglected. Schmidt (2007) and Koch (2011a,b) determine the maximum absolute value of the wavelet coefficients for each level of resolution and neglect the coefficients with absolute values smaller than a chosen percentage of the maximum value. This method and three additional ones are applied here and checked by computing the root mean square (rms) difference between the signals computed with and without data compression. The rms difference must not surpass the standard deviation with which the B-spline surface is fitted to the measurements. Otherwise, the data compression gives distorted results. However the question arises, which ratio between the standard deviation of the fit and the rms difference of a certain level of resolution should be selected. This is investigated here for a two-dimensional multi-scale representation. To obtain an objective method for neglecting wavelet coefficients, their confidence intervals are computed by Monte Carlo simulations and the coefficients to be neglected are determined by hypothesis tests.

The paper is organized as follows: Section 2 presents the two-dimensional multi-scale representation of signals. Section 3 covers the Monte Carlo method and the hypothesis tests of the wavelet coefficients. Section 4 discusses thresholds for the data compression which are applied to an example. The heights with respect to a plane of a concrete beam are measured by the laser scanner Leica HDS 3000 with a high density because of the edges.

2 TWO-DIMENSIONAL MULTI-SCALE REPRESENTATION OF SIGNALS

The tensor product of B-splines can be expressed by the Kronecker product which is well suited for deriving the n-dimensional multi-scale representation of signals. The Kronecker product does not lead to efficient formulas for computing if its definition is used. However for the two-dimensional case, the Kronecker product can be replaced by a matrix product (Koch, 2011b), which may be efficiently computed. In the following for easy reference, the formulas for the two-dimensional multi-scale representation are collected.

A two-dimensional B-spline surface depends on two parameters which will be called ξ_1, ξ_2 . It is expressed by the tensor product of the two B-spline basis functions $N_{i,q_1}(\xi_1), N_{j,q_2}(\xi_2)$ of degrees q_1, q_2 with, cf. Piegl and Tiller (1997, p. 34), Koch (2009b),

$$\mathbf{s}(\xi_1, \xi_2) = \sum_{i=0}^{h_1-1} \sum_{j=0}^{h_2-1} N_{i,q_1}(\xi_1) N_{j,q_2}(\xi_2) \mathbf{p}_{i,j} \quad (1)$$

and

$$\mathbf{s}(\xi_1, \xi_2) = \begin{pmatrix} x_1(\xi_1) \\ x_2(\xi_2) \\ H_1(\xi_1, \xi_2) \\ H_2(\xi_1, \xi_2) \end{pmatrix} \quad (2)$$

where the 4×1 vector $\mathbf{s}(\xi_1, \xi_2)$ denotes a point on the B-spline surface with the two-dimensional rectangular or curvilinear coordinates x_1 and x_2 with x_1 depending only on ξ_1 and x_2 only on ξ_2 . It is therefore assumed that the measurements for determining the B-spline surface are arranged in grids defined by the x - and y -coordinates. The third and the fourth coordinates H_1 and H_2 are the two quantities to be represented by the surface. In the following example, H_1 will be the height of the surface with respect to the x_1, x_2 -plane and H_2 the intensity of the reflected laser beam of a point measured by a laser scanner. The points

$$\mathbf{p}_{h_1 b_2} = |x_{1h_1}, x_{2b_2}, H_{1h_1 b_2}, H_{2h_1 b_2}|^T \quad \text{with} \\ h_1 \in \{0, \dots, l_1 - 1\}, b_2 \in \{0, \dots, l_2 - 1\} \quad (3)$$

are the unknown control points, which the B-spline surface approximately follows. The B-spline basis functions $N_{iq}(\xi)$ are computed by the recursion formula of Cox (1972) and de Boor (1972). So-called knots are introduced as a sequence of nondecreasing real numbers in the interval $[0, 1]$. The first and the last knot have multiplicity of the degrees q_1, q_2 to obtain the property of endpoint-interpolation. The numbers h_1, b_2 of unknown control points depend on the numbers of knots for ξ_1, ξ_2 and on q_1, q_2 in (1).

The B-spline surface is fitted to the measured coordinates of points. Let the rectangular or curvilinear coordinates x_1, x_2 together with H_1 and H_2 of $e_1 \times e_2$ points $\mathbf{s}(\xi_{1a_1}, \xi_{2a_2})$ be given in a grid, where ξ_{1a_1} with $a_1 \in \{1, \dots, e_1\}$ and ξ_{2a_2} with $a_2 \in \{1, \dots, e_2\}$ denote the location parameters which shall be known. Eq. (1) then leads to a linear relation between the unknown control points $\mathbf{p}_{h_1 b_2}$ and the given points $\mathbf{s}(\xi_{1a_1}, \xi_{2a_2})$. The observation equations for estimating $\mathbf{p}_{h_1 b_2}$ in a linear model are therefore given by

$$\sum_{h_1=0}^{l_1-1} \sum_{b_2=0}^{l_2-1} N_{h_1 q_1}(\xi_{1a_1}) N_{b_2 q_2}(\xi_{2a_2}) \mathbf{p}_{h_1 b_2} \\ = \mathbf{s}(\xi_{1a_1}, \xi_{2a_2}) + \mathbf{e}(\xi_{1a_1}, \xi_{2a_2}),$$

$$a_1 \in \{1, \dots, e_1\}, a_2 \in \{1, \dots, e_2\} \quad (4)$$

where $\mathbf{e}(\xi_{1a_1}, \xi_{2a_2})$ denotes the vector of errors of $\mathbf{s}(\xi_{1a_1}, \xi_{2a_2})$. There are $e_1 \times e_2$ linear equations for determining $l_1 \times l_2$ unknown control points so that $e_1 \times e_2 \geq l_1 \times l_2$ must hold.

Since the measured points are given in a grid, the lofting method by cross-sectional curve fits is applied. It is more efficient than the simultaneous estimation and gives identical results (Koch, 2009a). Eq. (4) is therefore rewritten by

$$\sum_{h_1=0}^{l_1-1} N_{h_1 q_1}(\xi_{1a_1}) \mathbf{b}_{h_1 a_2} = \mathbf{s}(\xi_{1a_1}, \xi_{2a_2}) + \mathbf{e}(\xi_{1a_1}, \xi_{2a_2}) \quad (5)$$

with

$$\sum_{b_2=0}^{l_2-1} N_{b_2 q_2}(\xi_{2a_2}) \mathbf{p}_{h_1 b_2} = \mathbf{b}_{h_1 a_2} \quad (6)$$

where $\mathbf{b}_{h_1 a_2}$ denotes the 4×1 vectors of control points of the isoparametric curves $\mathbf{s}(\xi_1, \xi_2 = \text{const})$ and $\mathbf{p}_{h_1 b_2}$ the control points of the isoparametric curves $\mathbf{s}(\xi_1 = \text{const}, \xi_2)$.

The control points $\mathbf{b}_{h_1 a_2}$ are estimated first by means of the observation equations (5). They read in matrix notation

$$\mathbf{N}(\xi_1) \mathbf{B} = \mathbf{S} + \mathbf{E} \quad (7)$$

where the $e_1 \times l_1$ matrix $\mathbf{N}(\xi_1)$ of the B-spline basis functions is defined by

$$\mathbf{N}(\xi_1) = \begin{vmatrix} N_{0q_1}(\xi_{11}) & \dots & N_{l_1-1,q_1}(\xi_{11}) \\ \dots & \dots & \dots \\ N_{0q_1}(\xi_{1e_1}) & \dots & N_{l_1-1,q_1}(\xi_{1e_1}) \end{vmatrix} \quad (8)$$

and the $l_1 \times e_2$ matrix \mathbf{B} of control points by

$$\mathbf{B} = \begin{vmatrix} \mathbf{b}_{01} & \dots & \mathbf{b}_{0e_2} \\ \dots & \dots & \dots \\ \mathbf{b}_{l_1-1,1} & \dots & \mathbf{b}_{l_1-1,e_2} \end{vmatrix} \quad (9)$$

so that the scalar elements of $\mathbf{N}(\xi_1)$ are multiplied by the vector elements of \mathbf{B} . With

$$\mathbf{s}(\xi_{1a_1}, \xi_{2a_2}) = \mathbf{s}_{a_1 a_2} \quad (10)$$

the $e_1 \times e_2$ matrix \mathbf{S} of given points is introduced by

$$\mathbf{S} = \begin{vmatrix} \mathbf{s}_{11} & \dots & \mathbf{s}_{1e_2} \\ \dots & \dots & \dots \\ \mathbf{s}_{e_1 1} & \dots & \mathbf{s}_{e_1 e_2} \end{vmatrix}. \quad (11)$$

The $e_1 \times e_2$ matrix \mathbf{E} of errors is obtained with replacing \mathbf{s} by \mathbf{e} in (10) and (11).

Eq. (7) represents the observation equations of a multivariate linear model by which the control points $\mathbf{b}_{h_1 a_2}$ of the isoparametric curves $\mathbf{s}(\xi_1, \xi_2 = \text{const})$ are estimated e_2 times for each value of ξ_2 . The estimate $\hat{\mathbf{B}}$ of \mathbf{B} follows by, cf. Koch (1999, p. 241),

$$\hat{\mathbf{B}} = (\mathbf{N}(\xi_1)^T \mathbf{N}(\xi_1))^{-1} \mathbf{N}(\xi_1)^T \mathbf{S}. \quad (12)$$

The matrix $\mathbf{N}(\xi_1)$ has full column rank so that the matrix $\mathbf{N}(\xi_1)^T \mathbf{N}(\xi_1)$ of normal equations is regular if the points are given on grids.

In the next step, (6) is used as observation equations for estimating the unknown control points $\mathbf{p}_{h_1 b_2}$ of the isoparametric curves $\mathbf{s}(\xi_1 = \text{const}, \xi_2)$. Applying matrix notation we find

$$\mathbf{N}(\xi_2) \mathbf{D} = \hat{\mathbf{B}}^T + \mathbf{E}_{\hat{\mathbf{B}}^T} \quad (13)$$

where the $e_2 \times l_2$ matrix $\mathbf{N}(\xi_2)$ of the B-spline basis functions is defined as in (8). The $l_1 \times l_2$ matrix \mathbf{D} of unknown control points is given by

$$\mathbf{D} = \begin{vmatrix} \mathbf{p}_{00} & \dots & \mathbf{p}_{0,l_2-1} \\ \dots & \dots & \dots \\ \mathbf{p}_{l_1-1,0} & \dots & \mathbf{p}_{l_1-1,l_2-1} \end{vmatrix} \quad (14)$$

and $\mathbf{E}_{\hat{\mathbf{B}}^T}$ is the matrix of errors of $\hat{\mathbf{B}}^T$.

Eq. (13) represents the observation equations of a multivariate linear model by which the control points $\mathbf{p}_{i_1 i_2}$ of the isoparametric curves $\mathbf{s}(\xi_1 = \text{const}, \xi_2)$ are estimated l_1 times for each value of ξ_1 . The estimate $\hat{\mathbf{D}}^T$ of \mathbf{D}^T follows by

$$\hat{\mathbf{D}}^T = (\mathbf{N}(\xi_2)^T \mathbf{N}(\xi_2))^{-1} \mathbf{N}(\xi_2)^T \hat{\mathbf{B}}^T. \quad (15)$$

The matrix $\hat{\mathbf{E}}$ of residuals is obtained from (13) with the estimate $\hat{\mathbf{D}}$ by

$$\hat{\mathbf{B}}^T = \mathbf{N}(\xi_2) \hat{\mathbf{D}} \quad (16)$$

and from (7) by

$$\hat{\mathbf{E}} = \mathbf{N}(\xi_1) \hat{\mathbf{B}} - \mathbf{S}. \quad (17)$$

The estimate $\hat{\sigma}^2$ of the 4×1 vector σ^2 of the variance factors for each of the four coordinates x_1, x_2, H_1, H_2 follows from, cf. Koch (2007, p. 96),

$$\sigma^2 = \text{vec} \hat{\mathbf{E}}^T \text{vec} \hat{\mathbf{E}} / (e_1 e_2 - l_1 l_2). \quad (18)$$

By summing the squares of the residuals of these coordinates and dividing by the degrees of freedom, their variances are obtained (Koch, 2010a).

Surfaces with discontinuities such as edges have to be scanned by a dense grid of points. In order to preserve the high resolution of the measurements when extracting geometrical information from the B-spline surface, points on the surface are computed with a density higher than that of the measurements. Let the points on the fitted surface have the given location parameters ξ_{1w_1}, ξ_{2w_2} with $w_1 \in \{1, \dots, v_1\}, w_2 \in \{1, \dots, v_2\}$. They are collected in the $v_1 \times v_2$ matrix \mathbf{S}_w which is defined by replacing e_1, e_2 in (11) by v_1, v_2 . The matrix \mathbf{S}_w is computed with (13) and (7) by

$$\hat{\mathbf{B}}_w^T = \mathbf{N}(\xi_{2w_2}) \hat{\mathbf{D}} \quad (19)$$

and

$$\mathbf{S}_w = \mathbf{N}(\xi_{1w_1}) \hat{\mathbf{B}}_w \quad (20)$$

where the $v_1 \times l_1$ matrix $\mathbf{N}(\xi_{1w_1})$ and the $v_2 \times l_2$ matrix $\mathbf{N}(\xi_{2w_2})$ of B-spline basis functions are obtained correspondingly to (8).

The multi-scale representation of signals starts with a certain level $j \in \mathbb{N}_0$ of resolution and introduces scaling functions for which B-splines are used here. Thus, the scaling functions $\Phi_{j_1 i_1 q_1}(\xi_1)$ and $\Phi_{j_2 i_2 q_2}(\xi_2)$ of level j_1 and j_2 for ξ_1 and ξ_2 are identified with the B-spline basis functions in (1) which are now defined for level j_1 and j_2

$$\Phi_{j_1 i_1 q_1}(\xi_1) = N_{j_1 i_1 q_1}(\xi_1), \Phi_{j_2 i_2 q_2}(\xi_2) = N_{j_2 i_2 q_2}(\xi_2). \quad (21)$$

The number l_{j_1} and l_{j_2} of scaling functions are equal to the number of control points for the parameters ξ_1 and ξ_2 in (1). l_{j_1} and l_{j_2} are determined by

$$l_{j_1} = 2^{j_1} + q_1, l_{j_2} = 2^{j_2} + q_2 \quad (22)$$

and the level j of resolution by

$$j = \max(j_1, j_2). \quad (23)$$

The $l_{j_1} \times 1$ vector $\Phi_{j_1}(\xi_1)$ collects the scaling functions

$$\Phi_{j_1}(\xi_1) = |\Phi_{j_1 0 q_1}(\xi_1), \dots, \Phi_{j_1, l_{j_1} - 1, q_1}(\xi_1)|^T \quad (24)$$

and accordingly the $l_{j_2} \times 1$ vector $\Phi_{j_2}(\xi_2)$. The signal $\mathbf{s}_j(\xi_1, \xi_2)$ is obtained from (1) with the $l_{j_1} \times l_{j_2}$ matrix $\mathbf{D}_j = \mathbf{D}$, now referred to level j , of control points from (14), which are called scaling coefficients,

$$\mathbf{s}_j(\xi_1, \xi_2) = \Phi_{j_1}^T(\xi_1) \mathbf{D}_j \Phi_{j_2}(\xi_2). \quad (25)$$

The signals of the multi-scale representation are therefore points on the B-spline surface.

We introduce for level $j_1 - 1$ the wavelet function $\Psi_{j_1 - 1, l, q_1}(\xi_1)$ with $l \in \{0, 1, \dots, L_{j_1 - 1} - 1\}$, $L_{j_1 - 1} = l_{j_1} - l_{j_1 - 1}$ and the $L_{j_1 - 1} \times 1$ vector $\Psi_{j_1 - 1}(\xi_1)$ of wavelet functions

$$\Psi_{j_1 - 1}(\xi_1) = |\Psi_{j_1 - 1, 0, q_1}(\xi_1), \dots, \Psi_{j_1 - 1, L_{j_1 - 1} - 1, q_1}(\xi_1)|^T \quad (26)$$

and accordingly the $L_{j_2 - 1} \times 1$ vector $\Psi_{j_2 - 1}(\xi_2)$ of wavelet functions. The vector $\Phi_{j_1}(\xi_1)$ from (24) is transformed to the $l_{j_1 - 1} \times 1$ vector $\Phi_{j_1 - 1}(\xi_1)$ of the lower level $j_1 - 1$ by the $l_{j_1} \times l_{j_1 - 1}$ matrix \mathbf{P}_{j_1} of constants

$$\Phi_{j_1 - 1}^T(\xi_1) = \Phi_{j_1}^T(\xi_1) \mathbf{P}_{j_1}. \quad (27)$$

The $L_{j_1 - 1} \times 1$ vector $\Psi_{j_1 - 1}(\xi_1)$ of wavelet functions is computed by the $l_{j_1} \times L_{j_1 - 1}$ matrix \mathbf{Q}_{j_1} of constants

$$\Psi_{j_1 - 1}^T(\xi_1) = \Phi_{j_1}^T(\xi_1) \mathbf{Q}_{j_1}. \quad (28)$$

Correspondingly, the $l_{j_2 - 1} \times 1$ vector $\Phi_{j_2 - 1}(\xi_2)$ and the $L_{j_2 - 1} \times 1$ vector $\Psi_{j_2 - 1}(\xi_2)$ are transformed. Eqs. (27) and (28), which are called two-scale relations, are also applicable for transformations to lower levels than $j_1 - 1$ and $j_2 - 1$. The matrices \mathbf{P}_{j_1} and \mathbf{Q}_{j_1} are given for $j_1 \in \{1, 2, \dots\}$ and $q_1 \in \{1, 2, 3\}$ by Stollnitz et al. (1995b) who determined \mathbf{Q}_{j_1} by imposing special conditions. In case of a two-dimensional multi-scale representation, there are three detail signals so that the signal $\mathbf{s}_j(\xi_1, \xi_2)$ at level j follows from the smoothed signal $\mathbf{s}_{j-m}(\xi_1, \xi_2)$ at level $j - m$ and the detail signals $\mathbf{g}_{j-k}^1(\xi_1, \xi_2)$ to $\mathbf{g}_{j-k}^3(\xi_1, \xi_2)$ at level $j - k$ by

$$\begin{aligned} \mathbf{s}_j(\xi_1, \xi_2) = & \mathbf{s}_{j-m}(\xi_1, \xi_2) + \sum_{k=1}^m [\mathbf{g}_{j-k}^1(\xi_1, \xi_2) \\ & + \mathbf{g}_{j-k}^2(\xi_1, \xi_2) + \mathbf{g}_{j-k}^3(\xi_1, \xi_2)] \end{aligned} \quad (29)$$

with

$$\mathbf{s}_{j-m}(\xi_1, \xi_2) = \Phi_{j_1 - m}^T(\xi_1) \mathbf{D}_{j-m} \Phi_{j_2 - m}(\xi_2), \quad (30)$$

with the detail signals

$$\begin{aligned}
\mathbf{g}_{j-k}^1(\xi_1, \xi_2) &= \Phi_{j-k}^T(\xi_1) \mathbf{C}_{j-k}^1 \Psi_{j-k}(\xi_2) \\
\mathbf{g}_{j-k}^2(\xi_1, \xi_2) &= \Psi_{j-k}^T(\xi_1) \mathbf{C}_{j-k}^2 \Phi_{j-k}(\xi_2) \\
\mathbf{g}_{j-k}^3(\xi_1, \xi_2) &= \Psi_{j-k}^T(\xi_1) \mathbf{C}_{j-k}^3 \Psi_{j-k}(\xi_2)
\end{aligned} \quad (31)$$

and with m chosen to be

$$m = \min(j_1, j_2) . \quad (32)$$

The $l_{j-k} \times l_{j-k}$ matrix \mathbf{C}_{j-k}^1 , the $l_{j-k} \times l_{j-k}$ matrix \mathbf{C}_{j-k}^2 and the $l_{j-k} \times l_{j-k}$ matrix \mathbf{C}_{j-k}^3 contain as elements the 4×1 vectors of coordinates of the points which determine the detail signals. They are called wavelet coefficients. Thus, the signal $\mathbf{s}_j(\xi_1, \xi_2)$ is expressed by the low-pass filtered signal $\mathbf{s}_{j-m}(\xi_1, \xi_2)$ at level $j - m$ and by the sum of detail signals, which are band-pass filtered versions of $\mathbf{s}_j(\xi_1, \xi_2)$, from level $j - 1$ to level $j - m$. Some wavelet coefficients in $\mathbf{C}_{j-k}^1, \mathbf{C}_{j-k}^2, \mathbf{C}_{j-k}^3$ might be small so that they can be neglected to compress the data. The matrices of scaling and wavelet coefficients of the level $j - 1$ are obtained by the decomposition equations

$$\begin{vmatrix} \mathbf{D}_{j-1} & \mathbf{C}_{j-1}^1 \\ \mathbf{C}_{j-1}^2 & \mathbf{C}_{j-1}^3 \end{vmatrix} = \begin{vmatrix} \bar{\mathbf{P}}_j \\ \bar{\mathbf{Q}}_j \end{vmatrix} |\mathbf{D}_j| \bar{\mathbf{P}}_j^T, \bar{\mathbf{Q}}_j^T . \quad (33)$$

The $l_{j-1} \times l_j$ matrix $\bar{\mathbf{P}}_j$ and the $l_{j-1} \times l_j$ matrix $\bar{\mathbf{Q}}_j$ follow from the matrices \mathbf{P}_j and \mathbf{Q}_j in (27) and (28) by

$$\begin{vmatrix} \bar{\mathbf{P}}_j \\ \bar{\mathbf{Q}}_j \end{vmatrix} = |\mathbf{P}_j, \mathbf{Q}_j|^{-1} \quad (34)$$

and similarly $\bar{\mathbf{P}}_j$ and $\bar{\mathbf{Q}}_j$. The matrices of scaling and wavelet coefficients of the lower levels $j - 2$ to $j - m$ are computed accordingly. The multi-scale representation starts at level j with the estimate \mathbf{D}_j of the matrix of control points by (15) and ends, when the lowest level $j - m$ with m from (32) is reached.

The points on the B-spline surface arranged in a dense grid and collected in the $v_1 \times v_2$ matrix \mathbf{S}_w from (20) shall be determined by a multi-scale representation. The index j is now added, i. e. \mathbf{S}_{jw} , to indicate the level j of resolution. The given location parameters are again ξ_{1w_1}, ξ_{2w_2} with $w_1 \in \{1, \dots, v_1\}, w_2 \in \{1, \dots, v_2\}$. To compute \mathbf{S}_{jw} , (29) is applied in connection with (30) and (31). The matrices of B-spline basis functions are therefore needed which also get the index j for the level of resolution, thus with (8)

$$\mathbf{N}_j(\xi_{1w}) = \begin{vmatrix} N_{0q_1}(\xi_{11}) & \dots & N_{j-1,q_1}(\xi_{11}) \\ \dots & \dots & \dots \\ N_{0q_1}(\xi_{1v_1}) & \dots & N_{j-1,q_1}(\xi_{1v_1}) \end{vmatrix} \quad (35)$$

where $\mathbf{N}_j(\xi_{1w})$ is a $v_1 \times l_j$ matrix. It is transformed to the lower level $j - 1$ like in (27) by

$$\mathbf{N}_{j-1}(\xi_{1w}) = \mathbf{N}_j(\xi_{1w}) \mathbf{P}_j \quad (36)$$

where the $v_1 \times l_{j-1}$ matrix $\mathbf{N}_{j-1}(\xi_{1w})$ contains the B-spline basis functions of level $j - 1$. Accordingly, the $v_2 \times l_{j-1}$ matrix $\mathbf{N}_{j-1}(\xi_{2w})$ of B-spline basis functions is obtained.

In addition, the $v_1 \times l_{j-1}$ matrix $\mathbf{W}_{j-1}(\xi_{1w})$ of wavelet functions with $l_{j-1} = l_j - l_{j-1}$ results with (28) by

$$\mathbf{W}_{j-1}(\xi_{1w}) = \mathbf{N}_j(\xi_{1w}) \mathbf{Q}_j . \quad (37)$$

Entspannen Sie sich.
Ab jetzt wird vieles
schneller.

Entspannen Sie sich und schöpfen Sie gleichzeitig das Potential Ihrer Instrumente besser aus. Die neuen Leica Qualitätsdienste ermöglichen es Ihnen. Leica erweitert die Dienstleistungen rund um die Instrumente. Ob **Datensicherung** oder **Echtzeithilfe direkt im Feld** oder dem **eigenen Referenzdienst**: Unser Anspruch: Den besten Service für die besten Instrumente.

Die neuen Leica Dienste

Leica
Geosystems

Correspondingly, the $v_2 \times L_{j-1}$ matrix $\mathbf{W}_{j-1}(\xi_{2w})$ and the matrices of the lower levels of resolution are obtained. The points of level j on the B-spline surface in the $v_1 \times v_2$ matrix \mathbf{S}_{jw} are then computed by

$$\begin{aligned} \mathbf{S}_{jw} &= \mathbf{N}_{j-m}(\xi_{1w}) \mathbf{D}_{j-m} \mathbf{N}_{j-m}^T(\xi_{2w}) \\ &+ \sum_{k=1}^m [\mathbf{N}_{j-k}(\xi_{1w}) \mathbf{C}_{j-k}^1 \mathbf{W}_{j-k}^T(\xi_{2w}) \\ &+ \mathbf{W}_{j-k}(\xi_{1w}) \mathbf{C}_{j-k}^2 \mathbf{N}_{j-k}^T(\xi_{2w}) \\ &+ \mathbf{W}_{j-k}(\xi_{1w}) \mathbf{C}_{j-k}^3 \mathbf{W}_{j-k}^T(\xi_{2w})] . \end{aligned} \quad (38)$$

The matrices of scaling and wavelet coefficients follow from (33).

3 CONFIDENCE INTERVALS FOR WAVELET COEFFICIENTS BY MONTE CARLO SIMULATIONS

To determine the wavelet coefficients which can be neglected for a data compression, statistical hypothesis testing is applied. The hypothesis is formulated that a wavelet coefficient of a detail signal expressing the height of the B-spline surface is equal to zero. To accept or reject the hypothesis is decided by means of the confidence interval of a wavelet coefficient which is computed by Monte Carlo methods.

The variances and covariances of measurements are determined by repetitions in a special multivariate linear model, cf. Koch (1999, p. 250). Experiences with estimating covariances have shown that the number of repetitions should surpass the number of covariances to be estimated by a factor of about 1.3 (Koch, 2010b). Even for scanning a small object with a high density of points like in the following example, we get 40 000 coordinates. This makes it prohibitive to repeat the measurements so frequently as to estimate the covariances. We therefore assume independent observations and estimate the variances only. This gives confidence intervals which are shorter than the ones with considering covariances (Koch, 2010b). However, it is acceptable because neglecting wavelet coefficients introduces approximations.

According to (2), (4) and (10), the four coordinates x_1, x_2, H_1, H_2 of the $e_1 \times e_2$ points $\mathbf{s}_{a_1 a_2}$ with $a_1 \in \{1, \dots, e_1\}, a_2 \in \{1, \dots, e_2\}$ have been measured to determine and to depict the B-spline surface. Let n_w be the number of repetitions with which x_1, x_2, H_1 are measured and $x_{w1 a_1 a_2}$ with $w \in \{1, \dots, n_w\}$ a repeated measurement of the x_1 -coordinate. Its mean value $\bar{x}_{1 a_1 a_2}$ is estimated by

$$\begin{aligned} \bar{x}_{1 a_1 a_2} &= \frac{1}{n_w} \sum_{w=1}^{n_w} x_{w1 a_1 a_2} \quad \text{for} \\ a_1 &\in \{1, \dots, e_1\}, a_2 \in \{1, \dots, e_2\} \end{aligned} \quad (39)$$

and accordingly $\bar{x}_{2 a_1 a_2}$ and $\bar{H}_{1 a_1 a_2}$. The estimated variances $\hat{\sigma}_{x_1 a_1 a_2}^2$ of the x_1 -coordinates follow from

$$\hat{\sigma}_{x_1 a_1 a_2}^2 = \frac{1}{n_w - 1} \sum_{w=1}^{n_w} (x_{w1 a_1 a_2} - \bar{x}_{1 a_1 a_2})^2, \quad (40)$$

the standard deviations from $\hat{\sigma}_{x_1 a_1 a_2} = (\hat{\sigma}_{x_1 a_1 a_2}^2)^{1/2}$ and accordingly $\hat{\sigma}_{x_2 a_1 a_2}$ and $\hat{\sigma}_{H_1 a_1 a_2}$. Taking the mean of the variances of the coordinates over the $e_1 \times e_2$ points gives the mean variance $\hat{\sigma}_{x_1}^2$ of the x_1 -coordinates

$$\hat{\sigma}_{x_1}^2 = \hat{\sigma}_{x_1 a_1 a_2}^2 / (e_1 e_2) \quad (41)$$

and accordingly $\hat{\sigma}_{x_2}^2, \hat{\sigma}_{H_1}^2$ and the standard deviations $\hat{\sigma}_{x_1}, \hat{\sigma}_{x_2}, \hat{\sigma}_{H_1}$. We assume the measured coordinates x_1, x_2, H_1 to be independently normally distributed and generate m_i random samples $x_{i1 a_1 a_2}$ with $i \in \{1, \dots, m_i\}$ for x_1 by, cf. Koch (2007, p. 197),

$$\begin{aligned} x_{i1 a_1 a_2} &= \hat{\sigma}_{x_1 a_1 a_2} z_i + \bar{x}_{1 a_1 a_2} \quad \text{for} \\ i &\in \{1, \dots, m_i\}, a_1 \in \{1, \dots, e_1\}, a_2 \in \{1, \dots, e_2\} \end{aligned} \quad (42)$$

with z_i being a random variate from the standard normal distribution $N(0, 1)$. Correspondingly, m_i random variates $x_{i2 a_1 a_2}$ and $H_{i1 a_1 a_2}$ are generated. The $l_{j_1} \times l_{j_2}$ scaling coefficients of the matrix $\hat{\mathbf{D}}_j$ at level j are estimated m_i times with these random variates by (15) so that m_i B-spline surfaces are fitted to the generated coordinates. The multi-scale representation of the points \mathbf{S}_{jw} on the surface starts according to (38) with level $j - 1$ and m_i matrices of scaling coefficients \mathbf{D}_{j-1} and m_i matrices of wavelet coefficients $\mathbf{C}_{j-1}^1, \mathbf{C}_{j-1}^2, \mathbf{C}_{j-1}^3$ are computed by (33). The multi-scale representation continues with level $j - 2$ and ends at level $j - m$ with m from (32).

We compute the confidence intervals of the wavelet coefficients which determine the heights H_1 of the B-spline surface. Let these wavelet coefficients of the matrices $\mathbf{C}_{j-k}^1, \mathbf{C}_{j-k}^2, \mathbf{C}_{j-k}^3$ for level $j - k$ be collected in the vector \mathbf{c}_{j-k} , for which m_i random variates $\mathbf{c}_{i,j-k}$ have been determined. The $1 - \alpha$ Bayesian confidence region C_B for \mathbf{c}_{j-k} is given by, cf. Koch (2007, p. 71),

$$P(\mathbf{c}_{j-k} \in C_B) = \int_{C_B} p(\mathbf{c}_{j-k}) d\mathbf{c}_{j-k} = 1 - \alpha \quad (43)$$

with

$$p(\mathbf{c}_{a,j-k}) \geq p(\mathbf{c}_{b,j-k}) \quad \text{for} \quad \mathbf{c}_{a,j-k} \in C_B, \mathbf{c}_{b,j-k} \notin C_B \quad (44)$$

where $p(\mathbf{c}_{j-k})$ is determined by the random variates $\mathbf{c}_{i,j-k}$ of \mathbf{c}_{j-k} . To test the null hypothesis

$$H_0 : \mathbf{c}_{j-k} = \mathbf{0} \quad \text{versus} \quad H_1 : \mathbf{c}_{j-k} \neq \mathbf{0}, \quad (45)$$

we use the confidence region C_B defined by (43) and (44). H_0 is accepted, if the value $\mathbf{0}$ lies within C_B . Otherwise, the hypothesis is rejected, cf. Koch (2007, p. 82). To determine the confidence interval for one component of \mathbf{c}_{j-k} , the probability of the component lying within a cell of suitable width is computed by the relative frequency. The probability at both ends of the histogram is added such that (44) is fulfilled until the probability α is reached. For m_i random variates, $m_i - 1$ cells are chosen (Koch, 2010b).

4 THRESHOLDS FOR DATA COMPRESSION

Thresholds for data compression by a multi-scale representation of signals are discussed for an example. Rectangular coordinates of points on the surface of a concrete beam under the ceiling of a basement are measured by the laser scanner Leica HDS 3000 in its local coordinate system. The origin lies in the center of the instrument, the z -axis points to the zenith, the y -axis coincides with the center of lines of sight of the instrument and the x -axis is perpendicular to y and z . Because of the edges of the concrete beam and of the ceiling, the points are scanned with a high density. The coordinates of 100 points parallel to the z -axis are measured with coordinate differences of about 6 mm and 100 points parallel the x -axis with the same differences. The y -coordinates vary between $4.01 \text{ m} \leq y \leq 6.45 \text{ m}$.

The B-spline surface (1) is fitted to the measured coordinates by applying the lofting method (15) to estimate the unknown control points. The coordinate x_1 in (2) is identical with the x -coordinate of the laser scanner, x_2 is equal to the z -coordinate and the height H_1 is obtained by $y_m - y$ with y_m being the maximum value of the y -coordinate. The coordinate H_2 follows from the intensity of the reflected laser beam of a point measured by the laser scanner. We set $q_1 = q_2 = 3$ in (4) for a smooth fit and choose the resolution levels $j_1 = j_2 = 6$ for ξ_1 and ξ_2 , thus $j = 6$ from (23). The numbers l_j and l'_j of unknown control points, i. e. scaling coefficients, then follow with $l_j = l'_j = 67$ from (22). In addition to fitting the B-spline surface to the 100×100 heights H_1 , a B-spline surface with the same parameters is also fitted to the intensities H_2 . The measured points plus residuals from (17) are depicted in Fig. 1 by their intensities plus residuals. The colors of the intensities result from the software 'Cyclone 7.1' of the Leica HDS 3000. It is obvious from Fig. 1 that the density of the measured points is sufficient to represent the edges of the concrete beam and the edge of the ceiling.

The standard deviation $\hat{\sigma}_{H_1}$ of the heights H_1 , which results from the variance factor (18) of the fit of the B-spline surface to the measured heights H_1 , follows with

$$\hat{\sigma}_{H_1} = 2.23 \text{ mm} . \quad (46)$$

To compute the variances of the measurements, the scans of the concrete beam under the ceiling have been repeated $n_w = 20$ times. These repetitions give a mean standard deviation $\hat{\sigma}_{H_1}$ by (41) of

$$\hat{\sigma}_{H_1} = 2.13 \text{ mm} . \quad (47)$$

This value agrees well with (46) and shows that the B-spline surface is fitted to the heights H_1 with a standard deviation which approximates the standard deviation of the measurements.

To preserve the resolution from the high density of the measurements, a grid of $v_1 \times v_2 = 210 \times 210$ points on the fitted surface is computed by (20), which is more than the two-fold of the density of the measurements. The results are shown in Fig. 2, which is enlarged in comparison to Fig. 1. Its orientation is slightly changed and only the upper right part of the concrete beam is depicted. The edges of the concrete beam are now visible in more detail than in Fig. 1.

As mentioned, a high density of the scans is needed because of the edges of the concrete beam and the ceiling. Apart from the edges, there are approximately planar surfaces. A high redundancy of information therefore exists in the B-spline representation of the concrete beam so that it should be compressed. The B-spline surface is estimated for the resolution level $j = 6$, the multi-scale representation therefore starts according to (29) with level $j = 5$ and ends with $j = 0$ because of $m = 6$ from (32). The number of scaling and wavelet coefficients for the different levels are presented in Table 1. It also shows the maximum absolute values of the wavelet coefficients for H_1 .

A multi-scale representation is computed by (38) for the dense grid of 210×210 points partly shown in Fig. 2. For the Monte Carlo simulations, m_i random variates are generated by (42) and m_i matrices $\mathbf{C}_{j-k}^1, \mathbf{C}_{j-k}^2, \mathbf{C}_{j-k}^3$ of wavelet coefficients for each level $j - k$ in (38) are computed. The random variates for the wavelet coefficients for H_1 are collected in the vectors $\mathbf{c}_{i,j-k}$ and for each coefficient the null hypothesis (45) is tested with $1 - \alpha = 0.95$ in (43). Accepting the hypothesis means that the wavelet coefficient does not significantly differ from zero so that it can be neglected. A threshold for the data compression is therefore established by the confidence interval. The number of eliminated wavelet coefficients thus obtained are given under method 1) in Table 2. It shows that 2 915 wavelet coefficients of the 3 264 of Table 1 can be neglected for level $j = 5$ which is 89.3 % of 3 264. For level $j = 4$ 424 coefficients or 49.1 % of 864 can be eliminated. Only a few coefficients are negligible for the levels $j = 3$ and $j = 2$. This is reasonable because high frequencies model the edges and are not needed to represent the planes.

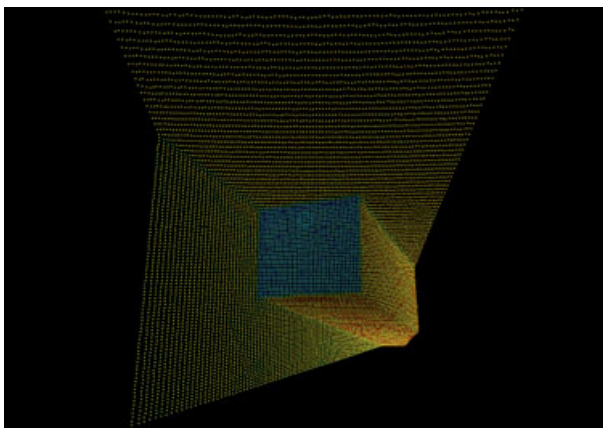


Fig. 1 | 100×100 measured points plus residuals depicted by intensities plus residuals of the B-spline surface fit

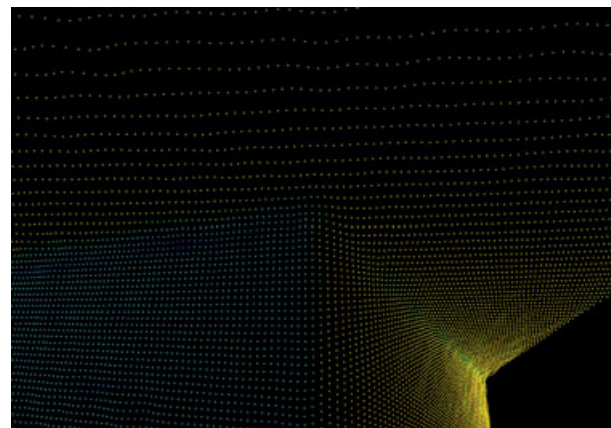


Fig. 2 | Part of the 210×210 computed points with intensities on the fitted B-spline surface

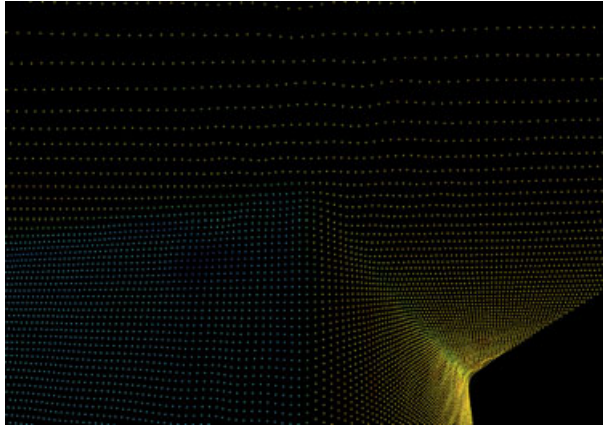


Fig. 3 | Part of the 210 × 210 computed points with intensities on the fitted B-spline surface after data compression by confidence intervals at levels $j = 5$ and $j = 4$

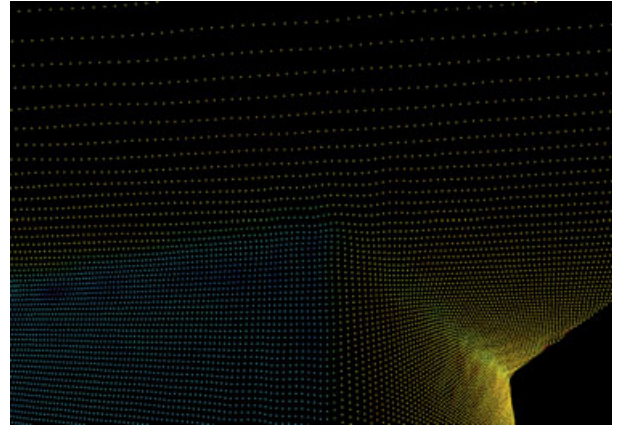


Fig. 4 | Part of the 210 × 210 computed points with intensities on the fitted B-spline surface after data compression by identical rms differences at level $j = 5$

A number of $m_j = 100\,000$ is recommended to compute confidence intervals with at least two significant digits (Koch, 2008). Numerical tests have shown that for detecting negligible wavelet coefficients $m_j = 50\,000$ is a sufficiently large number.

The coordinates of the grid of 210×210 points are computed for the levels $j = 5$ to $j = 0$ with all wavelet coefficients and with the coefficients minus the neglected ones. The rms differences of the heights H_1 are computed and shown under method 1) in Table 2. It is 1.50 mm for level $j = 5$ so that the ratio of $\hat{\sigma}_{H_1}$ from (46) to the rms value is $2.23\text{ mm}/1.50\text{ mm} = 1.49$. This ratio has to be greater than one, otherwise the data compression distorts the results. The ratio is $2.23\text{ mm}/1.66\text{ mm} = 1.34$ for level $j = 4$. For a rigorous data compression the levels $j = 5$ and $j = 4$ are chosen. Thus, $2\,915 + 424 = 3\,339$ wavelet coefficients are neglected which is 74.4% of the 4 489 scaling coefficients of level $j = 6$ in Table 1.

Level j	6	5	4	3	2	1	0
scaling coefficients	4 489	1 225	361	121	49	25	16
wavelet coefficients		3 264	864	240	72	24	9
max. abs. wav. coeff. [mm]		5.1	14	38	58	128	1 215

Table 1 | Number of scaling and wavelet coefficients and maximum absolute values of wavelet coefficients for decreasing levels j

That means a considerable reduction. The resulting points on the fitted surface are shown in Fig. 3. Fig. 2 and Fig. 3 have approximately the same orientation and scale. A comparison shows that the positions of the points have slightly changed but the results of the data compression is acceptable. Not only the amount of a coefficient is considered but also its standard deviation, which determines the length of the confidence interval, when selecting the wavelet coefficients, which can be discarded, by confidence intervals. A simpler procedure for eliminating wavelet coefficients is obtained if the absolute maximum value of the coefficients are used. Let $m_{c_{j-k}}$ be the maximum value in the vector c_{j-k} of level $j - k$ in (43) to (45). The threshold t_{j-k} for eliminating a coefficient at level $j - k$ is then determined by

$$t_{j-k} = p_c m_{c_{j-k}} / 100 \tag{48}$$

where p_c denotes a chosen percentage. The values for $m_{c_{j-k}}$ are given in Table 1. The percentage p_c is now selected for each level $j = 5$ to $j = 0$ such that the neglected wavelet coefficients lead to rms differences which are equal to the rms differences of method 1) in Table 2. The number of neglected coefficients are presented under method 2) in Table 2. The comparison with method 1) shows that less coefficients are neglected because coefficients larger than the threshold but with large standard deviations are accepted.

Level j	5	4	3	2	1	0
1) neglected wavelet coeff. by confidence intervals rms differences in [mm]	2 915 1.50	424 1.66	13 1.67	2 1.67	0 1.67	0 1.67
2) neglected wavelet coeff. by rms diff. from 1) rms differences in [mm]	2 885 1.50	313 1.66	12 1.67	1 1.67	0 1.67	0 1.67
3) neglected wavelet coeff. by 14.4% of max. wav. coeff. rms differences in [mm]	2 915 1.54	751 3.00	182 6.07	50 10.0	12 15.4	1 16.8
4) neglected wavelet coeff. by identical rms diff. rms differences in [mm]	2 885 1.50	26 1.50	1 1.50	0 1.50	0 1.50	0 1.50

Table 2 | Number of neglected wavelet coefficients and rms differences of H_1 for decreasing levels j obtained by four different methods

The same percentage p_c in (48) for all levels $j = 5$ to $j = 0$ is now selected for discarding the wavelet coefficients. It is set to $p_c = 14.4\%$ to obtain the same number of 2 915 neglected coefficients for level $j = 5$ as in method 1). The results together with the rms differences for H_1 are given in Table 2 under method 3). Because of the increase of m_{c-k} in Table 1, the rms differences for H_1 increase rapidly and surpass already for level $j = 4$ the standard deviation $\hat{\sigma}_{H_1}$ in (46). The data compression therefore has to stop at level $j = 5$ for method 3).

An rms difference for H_1 of 1.50 mm is obtained with method 1) for level $j = 5$. If p_c in (48) is chosen such that for each level $j = 5$ to $j = 0$ the same rms value is obtained, one finds the neglected wavelet coefficients under method 4) in Table 2. Because of only 26 neglected coefficients at level $j = 4$, the data compression should stop at level $j = 5$ so that 2 885 wavelet coefficients are neglected which is 64.3% of the 4 489 scaling coefficients of level $j = 6$ in Table 1. The resulting points on the fitted surface are shown in Fig. 4, which also has approximately the same orientation and scale as Fig. 2. The results are very similar to ones of Fig. 3. The methods 3) and 4) are based on the rms difference for H_1 . To obtain the rms value, the ratio of $\hat{\sigma}_{H_1}$ to the rms value should be chosen close to 1.5 as for method 1) at level $j = 5$. This avoids that the data compression distorts the results. The rms value is then determined by $\hat{\sigma}_{H_1}/1.5$ and one can proceed as in method 3) or 4).

5 CONCLUSIONS

It has been shown that neglecting wavelet coefficients by means of their confidence intervals leads to a preferable method of data compression. However, due to the computer time needed for the Monte Carlo simulations, the application of this method is only practical in case of a restricted number of measurements. As an alternative, a percentage of the maximum absolute value of the wavelet coefficients can be used to determine the threshold for eliminating the coefficients. The ratio of the standard deviation, with which the B-spline surface is fitted to the measured heights, to the rms difference between the heights computed with and without data compression should be set close to 1.5. This gives the rms value and the percentage to be chosen as threshold. The procedure ensures that the data compression does not distort the points computed on the fitted B-spline surface.

Acknowledgment: The author is indebted to Ernst-Martin Blome for assistance with the measurements and the graphical depiction of the results.

REFERENCES

- [1] Chui, C.K., Quak, E. (1992): Wavelets on a bounded interval. In D. Braess and L.L. Schumaker, editors, Numerical Methods of Approximation Theory, Vol. 9, pages 53–75, Basel, Birkhäuser.
- [2] Cox, M.G. (1972): The numerical evaluation of B-splines. J Institute of Mathematical Applications, 10:134–149
- [3] Boor, C. de (1972): On calculating with B-splines. J Approximation Theory, 6:50–62
- [4] Hennes, M. (2009): Freiformflächenerfassung mit Lasertrackern – eine ergonomische Softwarelösung zur Reflektoroffsetkorrektur. Allgemeine Vermessungs-Nachrichten, 116:188–194

- [5] Koch, K.R. (1999): Parameter Estimation and Hypothesis Testing in Linear Models, 2nd Ed. Springer, Berlin
- [6] Koch, K.R. (2007): Introduction to Bayesian Statistics, 2nd Ed. Springer, Berlin
- [7] Koch, K.R. (2008): Evaluation of uncertainties in measurements by Monte Carlo simulations with an application for laserscanning. J Applied Geodesy, 2:67–77
- [8] Koch, K.R. (2009a): Identity of simultaneous estimates of control points and of their estimates by the lofting method for NURBS surface fitting. Int J Advanced Manufacturing Technology, 44:1175–1180
- [9] Koch, K.R. (2009b): Fitting free-form surfaces to laserscan data by NURBS. Allgemeine Vermessungs-Nachrichten, 116:134–140
- [10] Koch, K.R. (2009c): Uncertainty of NURBS surface fit by Monte Carlo simulations. J Applied Geodesy, 3:239–247
- [11] Koch, K.R. (2010a): NURBS surface with changing shape. Allgemeine Vermessungs-Nachrichten, 117:83–89
- [12] Koch, K.R. (2010b): Uncertainty of results of laser scanning data with correlated systematic effects by Monte Carlo methods. ZfV–Z Geodäsie, Geoinformation und Landmanagement, 135:376–385
- [13] Koch, K.R. (2011a): Data compression by multi-scale representation of signals. J Applied Geodesy, 5:1–12
- [14] Koch, K.R. (2011b): Digital images with 3D geometry from data compression by multi-scale representations of B-spline surfaces. J Geodetic Science, 1: 240–250
- [15] Koch, K.R.; Schmidt, M. (2011): N-dimensional B-spline surface estimated by lofting for locally improving IRI. J Geodetic Science, 1:41–51
- [16] Mallat, S.G. (1989): A theory for multiresolution signal decomposition: the wavelet representation. IEEE Trans Pattern Anal Machine Intell, 11:674–693
- [17] Piegl, L., Tiller, W. (1997): The NURBS Book, 2nd Ed. Springer, Berlin
- [18] Quak, E.; Weyrich, N. (1994): Decomposition and reconstruction algorithms for spline wavelets on a bounded interval. Applied and Computational Harmonic Analysis, 1:217–231
- [19] Schmidt, M. (2001): Grundprinzipien der Wavelet-Analyse und Anwendungen in der Geodäsie. Shaker, Aachen
- [20] Schmidt, M. (2007): Wavelet modelling in support of IRI. J Adv Space Res, 39:932–940
- [21] Schmidt, M. (2010): Towards a multi-scale representation of multi-dimensional signals. In Proceedings of the VII Hotine-Marussi Symposium, Rome, July 6–10, 2009, in press, Berlin, Springer
- [22] Schmidt, M., Bilitza, D.; Shum, C.K.; Zeilhofer, C. (2008): Regional 4-D modeling of the ionospheric electron density. J Adv Space Res, 42:782–790
- [23] Stollnitz, E.J., DeRose, T.D.; Salesin, D.H. (1995a): Wavelets for computer graphics: a primer, part 1. IEEE Computer Graphics and Applications, 15(3):76–84
- [24] Stollnitz, E.J., DeRose, T.D.; Salesin, D.H. (1995b): Wavelets for computer graphics: a primer, part 2. IEEE Computer Graphics and Applications, 15(4):75–85
- [25] Yang, P., Qian, X. (2007): A B-spline-based approach to heterogeneous objects design and analysis. Computer-Aided Design, 39:95–111
- [26] Zeilhofer, C. (2008): Multi-dimensional B-spline modeling of spatio-temporal ionospheric signals. Deutsche Geodätische Kommission, Reihe A, 123, München

Prof. Dr.-Ing., Dr.-Ing. E. h. mult.
Karl-Rudolf Koch (em.),

PROFESSUR FÜR THEORETISCHE GEODÄSIE
RHEINISCHE FRIEDRICH-WILHELMS-UNIVERSITÄT
BONN

Nussallee 17 | 53115 Bonn
E-Mail: koch@geod.uni-bonn.de



Manuskript | eingereicht: 16.3.2011 | Im Peer-Review Verfahren begutachtet